processes

MDPI

Article

Estimation of Shale Gas Reserves: A Modified Material Balance Equation and Numerical Simulation Study

Reda Abdel Azim [1,*], Saad Alatefi [2] and Ahmad Alkouh [2]

[1] Petroleum Engineering Department, American University of Kurdistan, Sumel 42003, Iraq
[2] Department of Petroleum Engineering Technology, College of Technological Studies, PAAET, P.O. Box 42325, Kuwait City 70654, Kuwait; se.alatefi@paaet.edu.kw (S.A.); ab.alkouh@paaet.edu.kw (A.A.)
* Correspondence: reda.abdulrasoul@auk.edu.krd

Abstract: This study presents a comprehensive material balance equation (MBE) to estimate the reserve of shale gas reservoirs including free and adsorbed gas volume. The presented material balance equation takes into account the effect of stress change, matrix shrinkage, water volume production and influx, and critical desorption pressure. The material balance equation is converted into a linear relationship between the reservoir production and expansion parameters used during the derivation procedures that include rock-fluid properties and production history data. The proposed straight line reserve evaluation technique yields a slope of original free and absorbed gas in organic matrix, while the y-intercept yields the volume of original free gas in the in-organic matrix. A field case study of shale gas located in Australia is presented. Results show that the proposed MBE and the corresponding straight line reserve evaluation technique are rational and competent in estimating the free gas and adsorbed gas volumes accurately with error less than 6% compared to the numerical simulation model presented in this study using an in-house simulator based on finite element technique and FORTRAN language. Hence, the presented technique in this study can be used as a quick and easy to use tool to accurately estimate the free and adsorbed gas reserves and to improve the development of the production strategies of shale gas reservoirs.

Keywords: shale gas; material balance equation; straight line; adsorbed gas; matrix shrinkage

Citation: Abdel Azim, R.; Alatefi, S.; Alkouh, A. Estimation of Shale Gas Reserves: A Modified Material Balance Equation and Numerical Simulation Study. *Processes* **2023**, *11*, 1746. https://doi.org/10.3390/pr11061746

Academic Editor: Junqian Li

Received: 8 May 2023
Revised: 29 May 2023
Accepted: 2 June 2023
Published: 7 June 2023

1. Introduction

Shale gas reservoirs play a vital role in supporting the future global energy needs due to the increasing demand for clean energy [1–8]. The performance of shale gas reservoirs depends on various reservoir rock properties that include flow absorption, desorption, reservoir complexities, and natural fracture apertures. In addition, the subsurface natural gas stored as free and adsorbed gas that makes up to 85% of the total gas reserve and the remaining volume are dissolved in formation water [9]. Unlike conventional gas reservoirs, the flow of shale gas reservoirs has a unique and complex flow behavior where different states of gas coexist in the pore spaces such as free gas in matrix and fracture systems; adsorbed gas mainly occurs in the organic matrix, and dissolved gas occurs in formation water and in organic-rich matter. Gas adsorption is the accumulation process of gas molecules on the matrix surface that takes place in the pore spaces as follows: physisorption (physical adsorption), where the gas molecules adhere to the adsorbent surface through physical forces such as van der Waals forces, and chemisorption (chemical adsorption) through bonds by electron sharing or transfer through the chemical and mineralogical composition of the shale rock [10,11]; chemisorption was not taken into account in this study. Moreover, it should be noted that the shale gas transport mechanism in micro/nano organic pores is different than that in classical gas reservoirs (i.e., the flow does not always follow classical Darcy flow behavior). Xu et al. (2017, 2018) [12–14] presents various experimental studies regarding the gas flow mechanisms in the fracture and matrix system of organic-rich

shale gas reservoirs. These studies show that the gas transport behavior in the shale matrix can be divided into three types of flow mechanisms: viscous flow, Knudsen diffusion, and surface diffusion; only viscous flow and Knudsen diffusion exist in the shale fractures since no adsorbed gas exists within the fracture system. Furthermore, as a result of the stress changes caused by the formation pressure decline during production, the shale gas formation becomes more compressed and its porosity decreases. This porosity reduction continues until the pressure reaches the critical desorption pressure where the adsorbed gas begins to desorb, leaving the matrix pores and causing an increase in porosity; this process is known as the matrix shrinkage (Harpalani et al. 1990, Miao et al. 2020, 2022) [15–17]. This unique behavior of the combined effect of stress sensitivity and matrix shrinkage has a great impact on the evaluation of shale gas reserves and production development plans.

Gas-in-place estimation is mainly based on analog, volumetric, and material balance equation (MBE) techniques. The quality of the geophysical data, the fluid–rock interaction data, the recovery mechanism, the stage of development, and the maturity or degree of depletion all have a significant role in the choice and accuracy of the correct approach to estimate reserves and resources. Early on in the field development process, volumetric and analog calculations were the only methods available for estimating reserves. The analog method has the lowest accuracy among all methods of reserve estimation and is usually used under limited amounts of available exploration well data. The volumetric method for estimating gas in place is based on the log and core analysis data of the reservoir: pressure, average reservoir porosity, average fluid saturation, reservoir thickness, and the initial gas formation volume factor. For shale gas reservoirs, the parameters of gas adsorption characteristics to calculate the adsorbed gas volume are also required [9]. The volume of gas adsorption in shale reservoirs is controlled by total organic carbon, clay mineral components, and shale thermal maturity [18]. Nevertheless, the volumetric method for gas-in-place estimation in shale gas reservoirs includes various uncertainties that affect the accuracy of the calculations, especially the fact that the adsorbed gas calculation is performed at the initial reservoir pressure, which ignores the effect of a pressure decrease on pore space variation that usually exists during the life span of shale gas reservoirs. On the other hand, material balance has wide applications in the reserve's estimation of shale gas reservoirs. King (1993) [19] was among the first to propose a material balance equation for estimating the volume of adsorbed and free gas of shale reservoirs under limited water influx; however, his work ignored the matrix shrinkage effect and involved an iteration process to calculate the pseudo-deviation gas factor. Williams et al. (2001) [20] presented a material balance equation for coalbed methane and shale gas reservoirs without considering the water and formation compressibilities. Ahmed et al. (2006) [21] modified the equation of Williams et al. (2001) by taking into account the water and formation compressibilities and the adsorption effect without the need for an iteration process; however, Ahmed's work still ignored the combined effects of stress sensitivity and matrix shrinkage. Zhang et al. (2013) [22] proposed a new material balance equation using the natural fracture system that includes fracture aperture and orientation. Shi et al. (2018a) [23] proposed a modified MBE based on pseudo-deviation factor that takes into account the gas desorption process and matrix shrinkage effects. However, the pseudo-deviation factor determination process is complex and requires an iteration process. Recently, (Meng et al., 2020, Shi et al., 2022, and Yang et al., 2022) [24–26] proposed modified material balance equations for shale gas reservoirs that take into account the critical desorption pressure, stress sensitivity, and the matrix shrinkage effects. However, the developed equations use the concept of a pseudo-deviation factor, which require an iteration process.

Accordingly, it can be concluded that the main challenge for shale gas reservoirs is to estimate the gas in place using a proper material balance equation. Moreover, it can be concluded that the existing MBE's either ignores some of the important shale gas reservoir parameters (such as stress sensitivity, matrix shrinkage, and critical desorption pressure) or it includes such important parameters but with an iterative calculation process. Therefore, this study is a continuation of work that was presented by (Azim et al., 2022) [9] to propose

a modified material balance equation for estimating the shale gas reserves by taking into account stress sensitivity during the production process of shale and porosity variation as well as the critical desorption pressure using a simple linear relationship between reservoir expansion and production terms without any need of a complex and iterative calculation process. The proposed material balance equation was derived and validated against production data that were collected from gas wells in a certain shale gas reservoir located in Australia. The next section of the presented study will show the procedures used for the modified material balance equation and its application to shale gas reservoirs to estimate the gas reserves, including the free and the adsorbed volume.

2. General Material Balance Equation of the Shale Gas Reservoir

This section presents the derivation of the modified material balance equation for the shale gas reservoir. The equation assumes that gas is stored as free, absorbed, and dissolved gas. However, as the volume of dissolved gas in formation water is insignificant compared to the volume of free and absorbed gas, its volume can be ignored [27]. Moreover, it is assumed that the production process is isothermal, natural fractures serve as pathways rather than storage spaces, and when the pressure falls below the critical desorption pressure, gas is subsequently released (desorbed) from organic matter and the shale is deformed due to the combined effects of stress changes and matrix shrinkage.

The shale gas material balance equation can be expressed as

Production = Expansion (including expansion in the shale gas reservoir)

The production term is expressed as

$$G_p\beta_{\mathrm{g}} + W_p\beta_w - W_i \tag{1}$$

where G_p, W_p, and W_i are the cumulative gas production, the cumulative water production, and the volume of water injection, respectively. G_p, W_p, and W_i are all in volume units of m^3. B_g and B_w are the gas and water formation volume factors, both measured in m^3/m^3.

The expansion term is defined as follows.

Expansion = volume change of inorganic matrix + volume change of organic matrix + desorbed gas volume + pore volume occupied by free gas—produced water.

2.1. The Total Pore Volume Changes of the Inorganic Matrix

In shale gas reservoirs, the volume of water and the pores of the inorganic matrix change as the reservoir pressure decreases. This change in volume equals the summation of the elastic reservoir pore space variation and formation water expansion.

The water and pore space expansion are expressed as follows.

The change in pore space volume can be expressed as

$$c_w = \frac{1}{v_p}\frac{\Delta v_p}{\Delta p} \tag{2}$$

where c_p is the pore space compressibility in MPa^{-1} and v_p is the pore space volume in m^3.

$$c_w = \frac{1}{v_w}\frac{\Delta v_w}{\Delta p} \tag{3}$$

where c_w is the water compressibility in MPa^{-1} and v_w is the formation water volume in m^3.

From Equations (2) and (3), the change in pore volume and water volume can be calculated as follows:

$$c_p\,\Delta p\,v_{\mathrm{p}} = \Delta v_{\mathrm{p}} \tag{4}$$

$$c_w\,\Delta p\,v_{\mathrm{w}} = \Delta v_w \tag{5}$$

The total volume change due to expansion is the summation of the reservoir pore space variation in Equation (4) and water expansion in Equation (5):

$$\Delta v_{exp} = c_w \, \Delta p \, v_{\mathrm{w}} + c_p \, \Delta p \, v_{\mathrm{p}} \tag{6}$$

The water volume can be defined as a function of water saturation (S_w) as follows:

$$v_w = s_w v_{\mathrm{p}} \tag{7}$$

Therefore, the total volume change is rewritten as

$$\Delta v_{exp} = c_w \, \Delta p \, s_w v_{\mathrm{p}} + c_p \, \Delta p \, v_{\mathrm{p}} = \Delta p \, v_p \left(c_w \, s_w + c_p \right) \tag{8}$$

The pore space volume can be replaced by the volume of free gas in place in the inorganic matrix (G_{inof}) as follows:

$$v_p = \frac{v_{\mathrm{g}}}{s_{\mathrm{gi}}} = \frac{G_{inof} \, \beta_{\mathrm{gi}}}{1 - s_{wi}} \tag{9}$$

where G_{inof} is the volume of free gas in place in the inorganic matrix in (m^3) and B_{gi} is the initial gas volume factor in m^3/m^3. Thus, the total water and pore space volume expansion is given by

$$\Delta v_{exp} = c_w \, \Delta p \, s_w v_{\mathrm{p}} + c_p \, \Delta p \, v_{\mathrm{p}} = \Delta p \, \frac{G_{inof} \, \beta_{\mathrm{gi}}}{1 - s_{wi}} \left(c_w \, s_w + c_p \right) \tag{10}$$

The free gas expansion in the pore space can be expressed as

$$G_{inof} \left(\beta_{\mathrm{g}} - \beta_{\mathrm{gi}} \right) \tag{11}$$

where G_{inof} is the free gas volume in inorganic matter and B_{gi} is the initial gas volume factor in m^3/m^3; B_g (m^3/m^3) is the gas volume factor at a certain pressure P.

2.2. The Volume Changes in the Organic Matrix

According to Plamer et al. (1998) [28], the shale deformation is described by using the effect of compression and matrix shrinkage as follows:

$$\frac{\phi_{sh}}{\phi_{ish}} = 1 + \frac{c_m}{\phi_{sh}} (P - P_i) + \frac{\xi_l}{\phi_{sh}} \left(\frac{K}{M} - 1 \right) \left(\frac{P}{P_L + P} - \frac{P_i}{P_L + P_i} \right) \tag{12}$$

where Φ_{sh} is the shale porosity at any reservoir pressure, Φ_{ish} is the initial shale porosity at the initial reservoir pressure (both dimensionless), C_m is the organic matter expansion factor, K is the bulk modulus (MPa), ξ_l is the volumetric strain change (dimensionless), M is the axial strain modulus (MPa), P_L is Langmuir's pressure (MPa), and V_L is the maximum amount of adsorbed gas (Langmuir's volume, m^3).

$$c_m = \frac{1}{M} - \left(\frac{K}{M} + 0.5 \right) \gamma \tag{13}$$

where γ is the solid compressibility of shale; K/M in Equation (13) is expressed in Equation (14):

$$\frac{K}{M} = \frac{1}{3} \left(\frac{1 + v}{1 - v} \right) \tag{14}$$

where ν is Poisson's ratio.

Here, γ, the solid compressibility of shale, can be neglected, so Equation (13) can be written as follows:

$$C_m = \frac{1}{M} \tag{15}$$

Equation (12) can be simplified as follows:

$$\varnothing_{sh} - \varnothing_{shi} = \frac{1}{M}(P - P_i) + \xi_l \left(\frac{1}{3} \left(\frac{1+v}{1-v} \right) - 1 \right) \left(\frac{P}{P_L + P} - \frac{P_i}{P_L + P_i} \right) \tag{16}$$

The total volume change of the organic matrix is given by

$$\Delta V_{sh} = \frac{G_{forg} \beta_{\mathrm{gi}}}{\varnothing_{sh}} \left\{ \frac{1}{M}(P - P_i) + \xi_l \left(\frac{1}{3} \left(\frac{1+v}{1-v} \right) - 1 \right) \left(\frac{P}{P_L + P} - \frac{P_i}{P_L + P_i} \right) \right\} \tag{17}$$

where G_{forg} is the free gas volume in the organic matrix in m^3 and B_{gi} is the initial gas volume factor in m^3/m^3.

2.3. The Desorbed Volume of Adsorbed Shale Gas

The volume of desorbed gas in organic pores is calculated as follows:

$$V_{des} = V_L V_b \rho_{sh} \frac{P}{P + P_L} \tag{18}$$

where V_b is the reservoir bulk volume (m^3), ρ_{sh} is the density of shale at the initial reservoir pressure, P is the reservoir pressure; P_L is Langmuir's pressure (MPa), and V_L is the maximum amount of adsorbed gas (Langmuir's volume, m^3).

The rate at which gas is desorbed into the matrix pore space can be expressed as follows:

$$-\frac{\partial V_{des}}{\partial t} = -V_L V_b \rho_{sh} \frac{1}{(P + P_L)^2} \frac{\partial P}{\partial t} \tag{19}$$

The desorbed gas volume is calculated as follows:

$$V_{des} = \frac{G_{forg} \beta_{\mathrm{gi}}}{\phi_{sh}} \rho_{sh} \beta_{\mathrm{g}} \left(\frac{V_L P_i}{P_i + P_L} - \frac{V_L P}{P + P_L} \right) \tag{20}$$

2.4. The General Material Balance Equation for the Shale Gas Reservoir

The summation of all derived volume changes given in Equations (9), (16), and (18) is used to write the general material balance equation for shale reservoirs as follows:

$$\begin{aligned} & G_p \beta_{\mathrm{g}} + W_p \beta_w - W_i \\ & = G_{inof} \left[(\beta_{\mathrm{g}} - \beta_{\mathrm{gi}}) + \Delta p \frac{\beta_{\mathrm{gi}}}{1 - S_{wi}} (c_w s_w + c_p) \right] \\ & + G_{forg} \left\{ \begin{array}{l} (\beta_{\mathrm{g}} - \beta_{\mathrm{gi}}) - \frac{\beta_{\mathrm{gi}}}{\phi_{sh}} \left\{ \begin{array}{l} \frac{1}{M}(P - P_i) + \\ \xi_l \left(\frac{1}{3} \left(\frac{1+v}{1-v} \right) - 1 \right) \left(\frac{P}{P_L + P} - \frac{P_i}{P_L + P_i} \right) \end{array} \right\} \\ + \frac{\beta_{\mathrm{gi}}}{\phi_{sh}} \rho_{sh} \beta_{\mathrm{g}} \left(\frac{V_L P_i}{P_i + P_L} - \frac{V_L P}{P + P_L} \right) \end{array} \right\} \end{aligned} \tag{21}$$

New parameters include F, E_g, and X, defined in Equations (22) to (24), where parameter F represents the production term, parameter E_g represents the expansion term in the inorganic matrix, and parameter X represents the expansion term in the organic matrix:

$$F = G_p \beta_{\mathrm{g}} + W_p \beta_w - W_i \tag{22}$$

$$X = \left\{ \begin{array}{c} (\beta_g - \beta_{gi}) - \frac{\beta_{gi}}{\varnothing_{sh}} \left\{ \frac{1}{M}(P - P_i) + \xi_l \left(\frac{1}{3} \left(\frac{1+v}{1-v} \right) - 1 \right) \left(\frac{P}{P_L+P} - \frac{P_i}{P_L+P_i} \right) \right\} \\ + \frac{\beta_{gi}}{\varnothing_{sh}} \rho_{sh} \beta_g \left(\frac{V_L P_i}{P_i+P_L} - \frac{V_L P}{P+P_L} \right) \end{array} \right\} \quad (23)$$

$$E_g = \left[(\beta_g - \beta_{gi}) + \Delta p \frac{\beta_{gi}}{1 - s_{wi}} \left(c_w s_w + c_p \right) \right] \quad (24)$$

Accordingly, Equation (21) can be rewritten in terms of the new parameters (F, E_g, and X):

$$\frac{F}{E_g} = G_{inof} + G_{forg} \frac{X}{E_g} \quad (25)$$

Equation (25) is a linear equation; the slope is the organic matrix free gas volume G_{forg}, and the intercept is the free gas volume of inorganic matter G_{inof}. Both can be obtained by means of linear fitting using the plot of F/E_g vs. X/E_g.

The calculation procedures of the proposed MBE are summarized as follows:

1. Determine the rock and fluid properties needed for the calculation including the following: initial water saturation, matrix compressibility, shale density, the Langmuir volume, the Langmuir pressure, shale porosity, module of elasticity, Poisson's ratio of shale, and the gas formation volume factor at different pressures based on the production history data.
2. Obtain the production history data including the reservoir pressure profile, cumulative gas production, cumulative water production, and water influx if available. Compute steps 3 to 5 for each cumulative production record.
3. Calculate parameter F (Equation (22)).
4. Calculate parameter X (Equation (23)).
5. Calculate parameter E_g (Equation (24)).
6. Plot (F/E_g) vs. (X/E_g). According to (Equation (25)), the plot is a linear relationship; the slope is the organic free gas volume (G_{forg}), and the intercept is the inorganic matter free gas volume (G_{inof}).
7. Calculate the volume change in inorganic matter (Equation (9)).
8. Calculate the volume change of the shale matrix (Equation (16)).
9. Calculate the volume change of adsorbed gas (Equation (18)).

In the following section, an application of the modified material balance equation in a shale gas reservoir located in Australia is presented with all required input parameters including static rock–fluid properties as well as the dynamic reservoir performance data.

3. Field Case Study and Results

3.1. Geological Setting

The studied shale gas reservoir field is located in South Australia, and the field is broadly sickle shaped with its longer axis running northwest–southeast (see Figure 1). The shale gas field basin extends for about 38 km in the east–west direction and a maximum of 18 km in the north–south direction and covers an area of about 458 km^2. The gas-bearing section is limited to the Permian age sediments, and the maximum thickness of the formation is 1250 m.

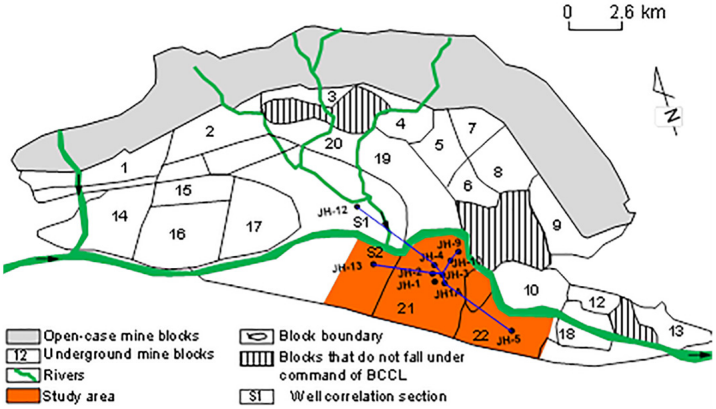

Figure 1. The geological map of the studied field.

3.2. Dynamic Poisson's Ratio and Young's Modulus for Shale Gas MBE

The dynamic Poisson ratio (v) and Young's modulus (ED) were calculated from sonic responses, i.e., the compressional and shear wave slowness (DTCO and DTSM) from DSI log data. There are two models to estimate geo-mechanical properties in the literature. Takahashi et al. (2007) [29] and Karacan (2009) [30] used the shear and compressional wave velocities. Al-Qahtani and Rahim (2001) [31] used the shear and compressional wave slowness. Our estimation models are based on equations from Al-Qahtani and Rahim, (2001). The dynamic shear modulus is calculated as follows:

$$G_d = 13474.45 \cdot \frac{RHOB}{DTSM^2} \tag{26}$$

where G_d is the shear modulus in GPa, $RHOB$ is the bulk density in g/cc, $DTSM$ is the shear wave slowness in µs/ft, and subscript d means dynamic.

Young's modulus is the ratio of applied stress to the longitudinal strain, and the bulk modulus is the inverse of bulk compressibility. They are calculated as follows:

$$ED = \frac{9G_d \cdot K_d}{3K_d + G_d} \tag{27}$$

$$K_d = 13474.45 \times RHOB \times \left(\frac{1}{DTCO^2}\right) - \frac{4G_d}{3} \tag{28}$$

where E_d is dynamic young's modulus in GPa, G_d is the dynamic shear modulus in GPa, K_d is the bulk modulus in GPa, $RHOB$ is the bulk density in g/cc, $DTCO$ is the compressional wave slowness in µs/ft, and subscript d is dynamic.

Poisson's ratio is the ratio of the fraction (or percent) of expansion divided by the fraction (or percent) of compression. It can also be calculated by shear and compressional wave slowness. The following equation was used to calculate the dynamic Poisson ratio [20]:

$$v = \frac{3K_d - 2G_d}{6K_d + 2G_d} \tag{29}$$

where ν is Poisson's ratio, K is the bulk modulus in GPa, G is the shear modulus in GPa, and subscript d is dynamic.

3.3. Log Interpretation Results of Geomechanical Properties

Figure 2 shows the logs and log interpretation results of porosity (PHIER and DPHI), permeability (PERMR), Young's modulus (E) and the Poisson ratio (v). PERMR is the permeability, RHOB is the bulk density log, PHIER is the total porosity under reservoir conditions, and DPHI is the density porosity.

The results show that DPHI is not reasonable at some depth because the wellbore's washout affects the logs' resistivity. Table 1 shows the averages of the interpreted PHIER, DPHI, and PERMR in well #JH1A. In well #JH1A, the PHIER, PERMR, and DPHI range from 0.38% to 1.60%, 0.08 mD to 6.34 mD, and 0.25% to 2.56%, respectively.

Young's modulus (E) normally increases with increasing depth and vice versa for Poisson's ratio (v). The average E in well# JH1A was 5.08 GPa. The average v ratio in well #JH1A was 0.31. Figure 3 shows the *RHOB* distribution across the reservoir volume in 3D space while Figure 4 shows the shale permeability distribution. It can be seen from Figure 4 that the permeability of the reservoir ranged from 0.00001 to 5 mD.

Table 1. Average properties of well #JH1A.

DEPTH (m)	RHOB (g/cc)	PHIER (%)	PERMR (mD)	DPHI (%)
505.77	1.35	1.60	6.34	1.06
572.07	1.40	0.95	4.86	0.56
617.68	1.42	1.02	3.65	0.53
685.72	1.37	1.20	2.58	0.49
774.00	1.43	0.75	1.81	0.19
909.10	1.46	0.41	0.61	0.17
983.52	1.52	0.55	1.33	0.64
1073.43	1.55	0.38	2.82	0.25
1106.15	1.42	0.67	0.08	2.56

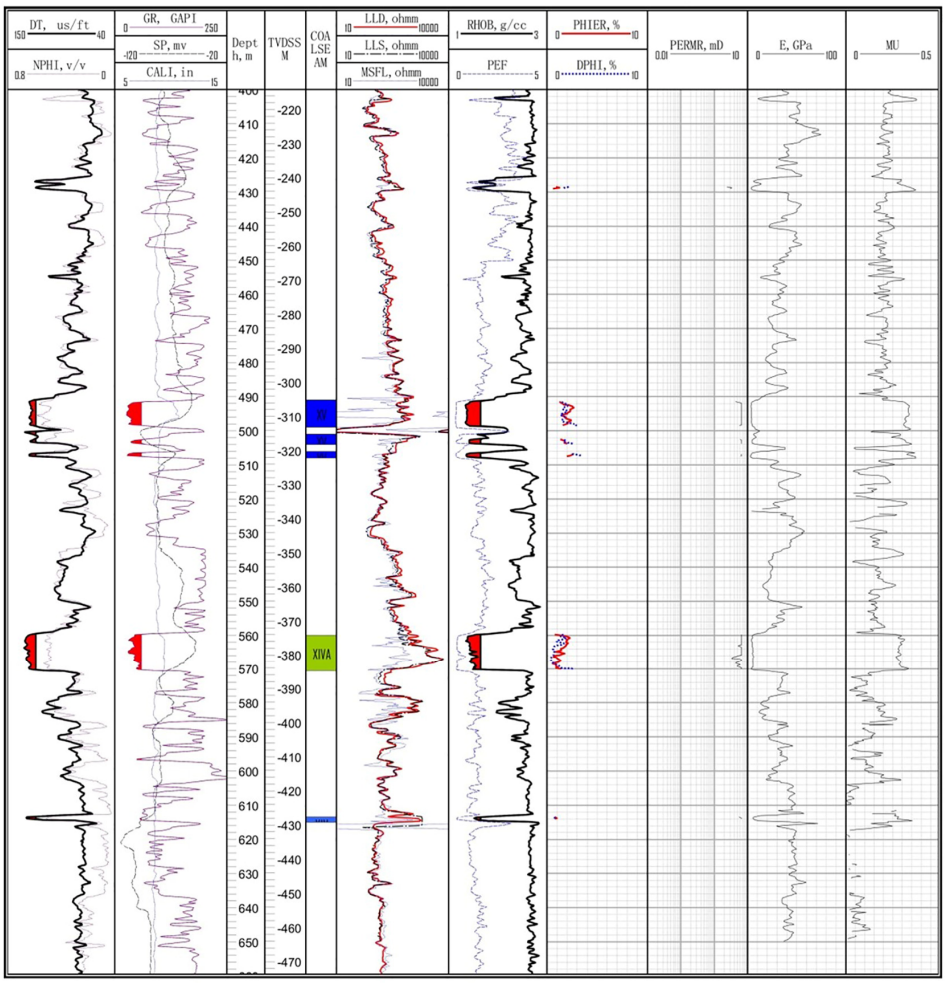

Figure 2. Logs and log interpretation of porosity, permeability, and static Young's modulus and Poisson's ratio of well #JH1A.

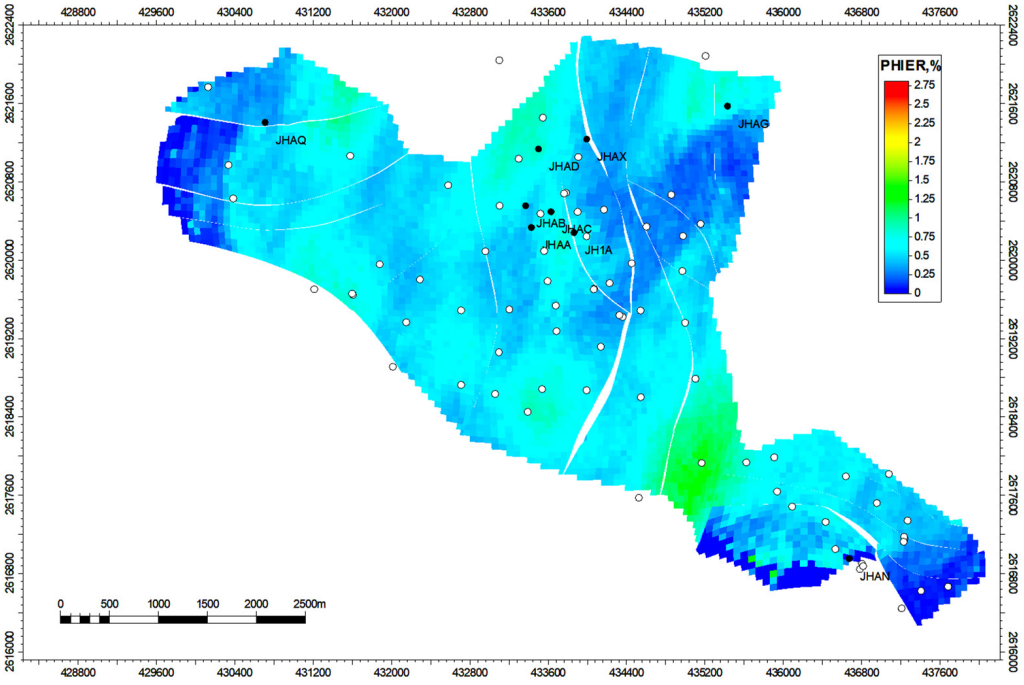

Figure 3. RHOB distribution in a 3D shale reservoir dynamic model.

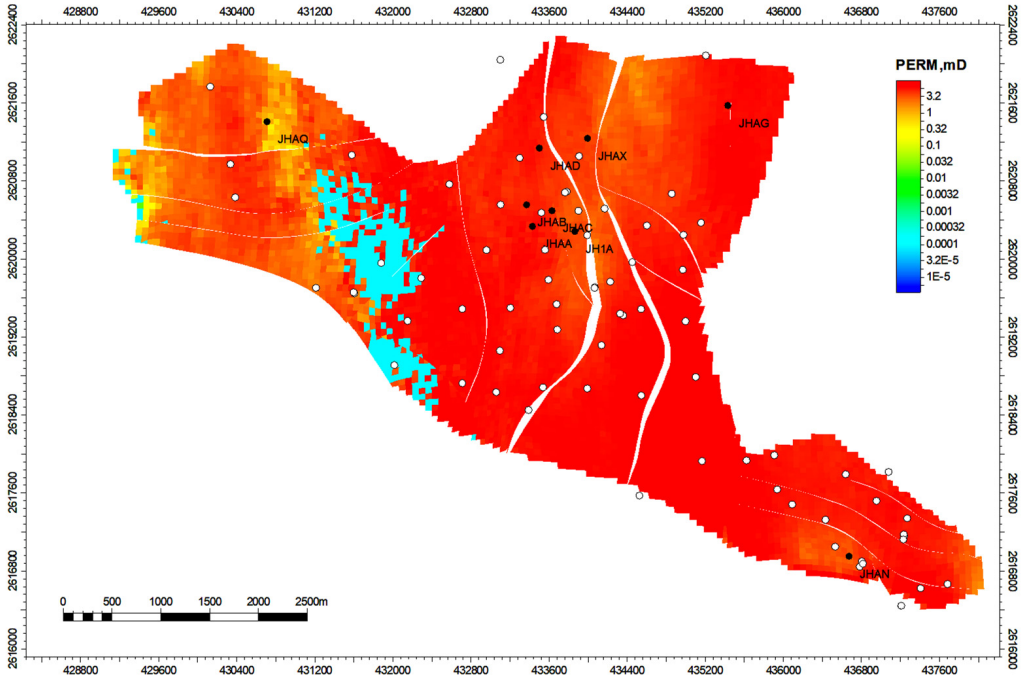

Figure 4. Permeability distribution in a 3D shale reservoir dynamic model.

Upon collection of the required data, the derived material balance equation in this study was applied to calculate the shale gas in place that included the free gas volume in both the organic and inorganic matrix and the volume of adsorbed gas in the organic pore space. In the presented case study, the gas was the only produced fluid considering that there was no flow back of the injected fluid of 5000 m^3 after the stimulation job. The reservoir parameters and production history data are presented in Tables 2 and 3.

Table 2. Reservoir rock and fluid properties for shale.

Rock/Fluid Property	Unit
Initial reservoir pressure Pi	26.9 MPa
Gas formation volume factor @ Pi	3.2×10^{-3} m^3/m^3
Inorganic matrix compressibility Cp	0.00245 MPa^{-1}
Initial water saturation in inorganic matter S_{wi}	0.24
Shale density φ_{sh}	2.0 t/m^3
Langmuir volume VL	41.95 m^3/t
Shale porosity	0.012
Langmuir pressure PL	24.8 MPa
Langmuir curve parameter match to volumetric strain	0.0158
Modulus of elasticity M	5800 MPa
Poisson's ratio of shale ν	0.31
Initial free gas in place from the dynamic (simulation) model	2.56×10^7 m^3

Table 3. Shale gas production history.

Pressure MPa	Cumulative Gas Production GP, m^3	Gas Volume Factor m^3/m^3
25.6	4,650,000	0.0035
23	6,024,000	0.0042
20.2	7,692,000	0.0053
17.35	10,902,000	0.0067
10.25	15,330,000	0.0105

The derived material balance equation was used to calculate the F, E_g, and X parameters for the determination of gas in place. Table 4 shows the calculation procedures, and Figure 5 presents the relationship between the production and reservoir expansion parameters. It is clear from Figure 5 that there is a linear relationship between the proposed production and expansion terms of the studied reservoir with a coefficient of determination of 0.97 (R^2 = 0.97). Accordingly, the calculated total initial free gas in place is equal to 2.4×10^7 m^3, which includes a free gas volume in shale (organic matrix) of 1.8×10^7 m^3 and a volume of 0.6×10^7 m^3 of free gas in the inorganic matrix. The error between the total free gas volume from the modified MBE and the dynamic reservoir model is 6.2%, which highlights the reliability of the presented MBE in calculating shale gas in place. Furthermore, it is important to note that the estimated free gas volume in shale was around 67% of the total gas in place, which is consistent with the notion that the majority of free gas in shale reservoirs exists in the organic pores of the organic-rich shale gas reservoirs [32]. Such results indicate that the proposed MBE can act as a quick and accurate reserve estimation tool for shale gas reservoirs, saving the computational time required for building and running dynamic simulation reservoir models.

Finally, it should be mentioned that the volume of adsorbed gas (G_A) of the studied shale reservoir was 0.0698×10^7 m^3, which was calculated using the following equation:

$$G_A = \frac{G_{forg}\beta_{gi}}{\varnothing_{sh}} \rho_{sh} \left(\frac{V_L P_i}{P_i + P_L} \right) \quad (30)$$

where G_{forg} is the free gas volume in the organic matrix in m^3, B_{gi} is the initial gas volume factor (m^3/m^3), *PL* is Langmuir's pressure (MPa), *VL* is the maximum amount of adsorbed gas (Langmuir's volume, m^3), and ρ_{sh} and φ_{sh} are the shale density (t/m^3) and the shale porosity (dimensionless), respectively.

Table 4. MBE equation calculation procedures.

Pressure (MPa)	Volume Change in Inorganic Matter Equation (9) (m^3)	Volume Change of the Shale Matrix Equation (16) (m^3)	Volume Change of Adsorbed Gas Equation (18) (m^3)	F	X	Eg
25.6	70.98	288.40	9063.44	14,019	0.000828	0.000784
23.0	138.65	546.78	20,315.88	21,506	0.001264	0.001121
20.2	249.55	962.60	44,652.25	32,922	0.001957	0.001682
17.35	429.25	1508.05	110,890.18	66,190	0.003849	0.003312
10.25	652.74	1925.06	349,892.54	172,828	0.010098	0.008458

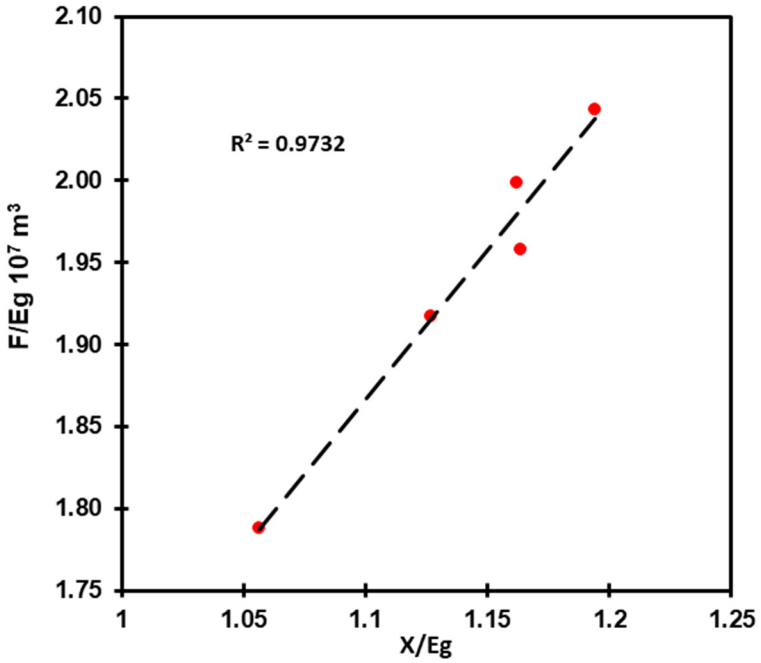

Figure 5. Linearization of the presented MBE in this study for shale gas reserve estimation.

4. Validation Using a Numerical Simulation Model

In this study, the fluid flow in shale gas reservoirs was simulated using an in-house finite element simulator. Herein, the finite element technique was used to discretize the fluid flow equation for single-phase flow in 2-D space.

The used continuity equation can be written as follows:

$$\frac{\partial}{\partial x}(\rho_g u_g) = -\frac{\partial}{\partial t}(\phi \rho_g) \tag{31}$$

where ρ_g *and* u_g are the gas density and velocity, respectively.

Introducing the gas formation volume factor and the source/sink term (q_g) into Equation (31) will give the following:

$$\frac{\partial}{\partial x}(\beta_g u_g) - q_g = -\frac{\partial}{\partial t}(\phi \beta_g) \tag{32}$$

Darcy's velocity is used in Equation (32), and the equation can be reformulated as

$$\frac{\partial}{\partial x}\left(\frac{c k_x \beta_g}{\mu_g}\frac{\partial p_g}{\partial x}\right) + q_g = \phi \frac{\partial p_g}{\partial t}\frac{\partial \beta_g}{\partial p_g} \tag{33}$$

For two-dimensional flow, Equation (33) can be written as

$$\frac{\partial}{\partial x}\left(\frac{ck_x\beta_g}{\mu_g}\frac{\partial p_g}{\partial x}\right)+\frac{\partial}{\partial z}\left(\frac{ck_z\beta_g}{\mu_g}\frac{\partial p_g}{\partial z}\right)+q_g=\phi\frac{\partial p_g}{\partial t}\frac{\partial \beta_g}{\partial p_g} \tag{34}$$

Using Equation (19), the amount of adsorbed gas can be treated as a source term (i.e., injection well) in Equation (34), and this can be written as

$$\frac{\partial}{\partial x}\left(\frac{ck_x\beta_g}{\mu_g}\frac{\partial p_g}{\partial x}\right)+\frac{\partial}{\partial z}\left(\frac{ck_z\beta_g}{\mu_g}\frac{\partial p_g}{\partial z}\right)+V_L\rho_R\frac{1}{(p+p_L)^2}\frac{\partial p}{\partial t}=\phi\frac{\partial p_g}{\partial t}\frac{\partial \beta_g}{\partial p_g} \tag{35}$$

The finite element technique can be used to discretize Equation (35) as follows:

$$\begin{aligned}\int_\Omega\left(\phi c_t {N_p}^T N_p d\Omega\right)\left(\overrightarrow{P}^i-\overrightarrow{P}^{i-1}\right)+\left(V_L\rho_R\tfrac{1}{(p+p_L)^2}{N_p}^T N_p d\Omega\right)\left(\overrightarrow{P}^i-\overrightarrow{P}^{i-1}\right)+\Delta t^i\left[\int_\Omega\left(\tfrac{ck_xB_g}{\mu}\tfrac{\partial {N_p}^T}{\partial x}\tfrac{\partial N_p}{\partial x}+\right)d\Omega\right]\overrightarrow{P}^i\\ +\Delta t^i\left[\int_\Omega\left(\tfrac{ck_zB_g}{\mu}\tfrac{\partial {N_p}^T}{\partial z}\tfrac{\partial N_p}{\partial z}\right)d\Omega\right]\overrightarrow{P}^i+\int_\Gamma {N_p}^T \mathrm{q}\,\mathrm{d}=0.0\end{aligned} \tag{36}$$

$$\overrightarrow{N}_p{}^T=(N_1N_2\cdots Nn) \tag{37}$$

$$\overrightarrow{N}_u=\begin{bmatrix}N_1 & 0 & N_1 & \cdots & 0\\ 0 & N_1 & 0 & \cdots & N_1\end{bmatrix} \tag{38}$$

N_p is the pressure shape function, n is the number of nodes, N_u is the displacement function, and P represents the pressure nodal values.

Galerkin's finite element technique is used to stabilize the solution of the flow equations as follows:

$$A\times(p)+s\times(p)+H\times(p)=0 \tag{39}$$

where

$$A=\int_{ve}[B]^T\left(k\frac{P_L}{(P_L+P)^2}\right)N_p dV \tag{40}$$

$$S=\int_{ve}\left[N_p\right]^T\left(\frac{\beta_g V_L P_L}{(P_L+P)^2}\right)N_p dV \tag{41}$$

$$H=\int_{ve}\left[\nabla N_p\right]^T\left(\frac{k}{\mu_g}\right)\nabla N_p dV \tag{42}$$

The established finite element model in this study was validated in Part I of this study [9] using the data provided in Table 2 with one horizontal hydraulic fracture in the presented shale reservoir simulation model. Figure 6 shows the 2-D model used with pressure and stress distribution around the wellbore. Figure 7 shows the gas pressure distribution across the horizontal hydraulic fracture and within the rock matrix. It can be seen from Figure 7 that the gas pressure is depleted immediately through the hydraulic fracture during the production process and is slowly depleted within the rock matrix as the result of low permeability.

The gas in place estimated by the simulation model is 2.65×10^7 m^3, which includes the free gas volume of 1.97×10^7 m^3 in shale and the free gas volume of 0.68×10^7 m^3 in the inorganic matrix, which is consistent with the results of the modified material balance equation presented earlier in Section 3.

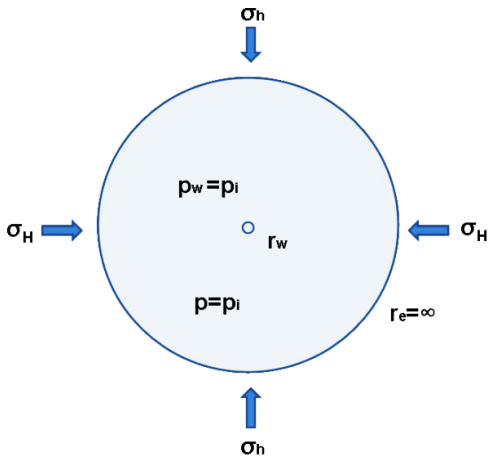

Figure 6. 2-D problem used for the simulation model.

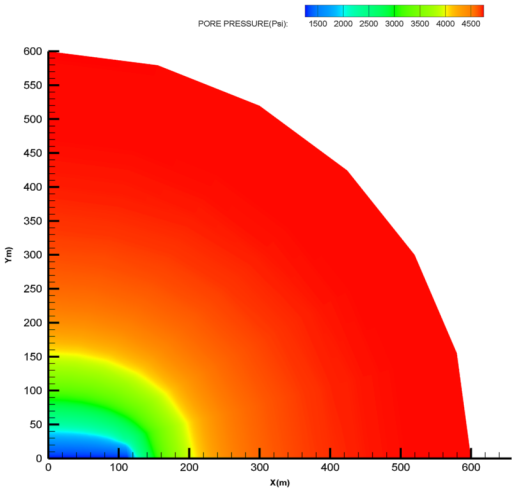

Figure 7. Gas pressure distribution around the hydraulic fracture and rock matrix.

5. Conclusions

The importance of accurate reserve estimation and production forecasting in shale gas reservoirs cannot be overstated. The shale gas material balance equation plays a crucial role in the estimation of recoverable reserves and production forecasting for such unconventional reservoirs. Furthermore, with the increasing demand for energy worldwide and the potential of shale gas resources to meet this demand, accurate estimates of recoverable reserves and production forecasting are essential for decision making in the energy industry. Therefore, this study presents a comprehensive derivation for a modified material balance (MBE) equation of shale gas reservoirs to accurately estimate the free and adsorbed gas in place. The presented equation accounts for the changes that occur in shale reservoirs during gas production including the variation in the pore space volume due to the combined effects of stress changes and matrix shrinkage, the effect of the critical desorption pressure in organic-rich matrix, and the volume of produced water and influx.

Real field data from a shale gas reservoir in Australia were used to test the proposed linear correlation in this study. The results demonstrate that the MBE estimate of total gas in place agrees well with the dynamic reservoir model results, with an average error of 6%, which highlights the reliability of the presented MBE in calculating shale gas in place.

The proposed MBE in this study can be used as a quick and easy to use tool to accurately describe the production characteristics of shale gas reservoirs and to appropriately estimate the free and adsorbed gas reserves and has significant applications for the development of the production strategies of shale gas reservoirs.

Author Contributions: Conceptualization, R.A.A. and S.A.; methodology, R.A.A.; software, R.A.A.; validation, R.A.A., S.A. and A.A.; formal analysis, R.A.A. and S.A.; investigation, R.A.A.; resources, A.A.; data curation, R.A.A.; writing—original draft preparation, R.A.A.; writing—review and editing, S.A. and A.A.; visualization, S.A.; supervision, R.A.A. All authors have read and agreed to the published version of the manuscript.

Funding: This research received no external funding.

Data Availability Statement: The datasets used and/or analyzed during the current study are available from the corresponding author upon reasonable request.

Conflicts of Interest: The authors declare no conflict of interest.

References

1. Feng, Z.; Dong, D.; Tian, J.; Qiu, Z.; Wu, W.; Zhang, C. Geochemical characteristics of Longmaxi Formation shale gas in the Weiyuan area, Sichuan Basin, China. *J. Pet. Sci. Eng.* **2018**, *167*, 538–548. [CrossRef]
2. Meng, X.; Chen, H.; Niu, F.; Tang, Y.; Yin, C.; Wu, F. Microseismic monitoring of stimulating shale gas reservoir in SW China: 1. An improved matching and locating technique for downhole monitoring. *J. Geo. Res.* **2018**, *123*, 1643–1658. [CrossRef]
3. Liu, H.; Meng, S.; Su, J.; Zhang, G.; Chen, L. Reflections and suggestions on the development and engineering management of shale gas fracturing technology in China. *Nat. Gas. J. B* **2019**, *6*, 539–545. [CrossRef]
4. Qiao, J.; Littke, R.; Zieger, L.; Jiang, Z.; Fink, R. Controls on gas storage characteristics of Upper Paleozoic shales from the southeastern Ordos Basin. *Mar. Pet. Geol. J.* **2020**, *117*, 104377. [CrossRef]
5. Sun, M.; Yu, B.; Hu, Q.; Zhang, Y.; Li, B.; Yang, R.; Melnichenko, Y.B.; Cheng, G. Pore characteristics of Longmaxi shale gas reservoir in the Northwest of Guizhou, China: Investigations using small-angle neutron scattering (SANS), helium pycnometry, and gas sorption isotherm. *Int. J. Coal Geo.* **2017**, *171*, 61–68. [CrossRef]
6. Sun, Z.; Li, X.; Shi, J.; Zhang, T.; Sun, F. Apparent permeability model for real gas transport through shale gas reservoirs considering water distribution characteristic. *Int. J. Heat* **2017**, *115*, 1008–1019. [CrossRef]
7. Li, Y.F.; Sun, W.; Liu, X.W.; Zhang, D.W.; Wang, Y.C.; Liu, Z.Y. Study of the relationship between fractures and highly productive shale gas zones, Longmaxi Formation, Jiaoshiba area in eastern Sichuan. *Pet. Sci. J.* **2018**, *15*, 498–509. [CrossRef]
8. Sun, F.; Yao, Y.; Li, G.; Li, X. A slip-flow model for multi-component shale gas transport in organic nanopores. *Ara. J. Geo.* **2019**, *12*, 143. [CrossRef]
9. Abdel Azim, R.; Aljehani, A. Finite Element and Neural Network Models to Forecast Gas Well Inflow Performance of Shale Reservoirs. *Processes* **2022**, *10*, 2602. [CrossRef]
10. Cheremisina, O.V.; Ponomareva, M.A.; Bolotov, V.A.; Osipov, A.S.; Sitko, A.V. Thermodynamic characteristics of the hydrogen sulfide sorption process by ferromanganese materials. *ACS Omega* **2022**, *7*, 3007–3015. [CrossRef]
11. Nazarenko, M.Y.; Saltykova, S.N.; Rudko, V.A.; Pihl, O. Production of isotropic coke from shale tar at various parameters of the delayed coking process. *ACS Omega* **2021**, *6*, 22173–22179. [CrossRef] [PubMed]
12. Xu, J.; Wu, K.; Yang, S.; Cao, J.; Chen, Z.; Pan, Y.; Yan, B. Real gas transport in tapered noncircular nanopores of shale rocks. *AIChE J. Am. Inst. Chem. Eng.* **2017**, *63*, 3224–3242. [CrossRef]
13. Xu, J.; Wu, K.; Li, R.; Li, Z.; Li, J.; Xu, Q.; Chen, Z. Real gas transport in shale matrix with fractal structures. *Fuel* **2018**, *219*, 353–363. [CrossRef]
14. Xu, J.; Wu, K.; Li, Z.; Pan, Y.; Li, R.; Li, J.; Chen, Z. A model for gas transport in dual-porosity shale rocks with fractal structures. *Ind. Eng. Chem. Res.* **2018**, *57*, 6530–6537. [CrossRef]
15. Harpalani, S.; Schraufnagel, R.A. Shrinkage of coal matrix with release of gas and its impact on permeability of coal. *Fuel. J.* **1990**, *69*, 551–556. [CrossRef]
16. Miao, Y.; Zhao, C.; Zhou, G. New rate-decline forecast approach for low-permeability gas reservoirs with hydraulic fracturing treatments. *J. Pet. Sci. Eng.* **2020**, *190*, 107112. [CrossRef]
17. Miao, Y.; Zhao, C.; Zhou, G. Gas flowrate evaluation in coal coupling the matrix shrinkage effect caused by water extraction. *J. Energy Resour. Technol.* **2022**, *144*, 032301. [CrossRef]
18. Mengal, S.A. Accounting for Adsorbed Gas and Its Effect on Production Bahavior of Shale Gas Reservoirs. Ph.D. Thesis, Texas A & M University, College Station, TX, USA, 2010; p. 5.
19. King, G.R. Material-balance techniques for coal-seam and devonian shale gas reservoirs with limited water influx. *SPE. Res. J.* **1993**, *8*, 67–72. [CrossRef]
20. Williams-Kovacs, J.D.; Clarkson, C.R.; Nobakht, M. Impact of material balance equation selection on rate-transient analysis of shale gas. In *SPE Annual Technical Conference and Exhibition*; OnePetro: Richardson, TX, USA, 2012. [CrossRef]
21. Ahmed, T.; Centilmen, A.; Roux, B. A generalized material balance equation for coalbed methane reservoirs. *SPE Annu. Tech. Conf. Exhib.* **2006**, *8*, 21–25.
22. Zhang, L.H.; Chen, G.; Zhao, Y.L.; Liu, Q.F.; Zhang, H.C. A modified material balance equation for shale gas reservoirs and a calculation method of shale gas reserves. *Gas Ind. J.* **2013**, *33*, 66–70.

23. Shi, J.; Chang, Y.; Wu, S.; Xiong, X.; Liu, C.; Feng, K. Development of material balance equations for coalbed methane reservoirs considering dewatering process, gas solubility, pore compressibility and matrix shrinkage. *Int. J. Coal Geol.* **2018**, *195*, 200–216. [CrossRef]
24. Meng, Y.; Li, M.; Xiong, X.; Liu, J.; Zhang, J.; Hua, J.; Zhang, Y. Material balance equation of shale gas reservoir considering stress sensitivity and matrix shrinkage. *Arab. J. Geosci.* **2020**, *13*, 535. [CrossRef]
25. Shi, J.-T.; Jia, Y.-R.; Zhang, L.-L.; Ji, C.-J.; Li, G.-F.; Xiong, X.-Y.; Huang, H.-X.; Li, X.-F.; Zhang, S.-A. The generalized method for estimating reserves of shale gas and coalbed methane reservoirs based on material balance equation. *Pet. Sci.* **2022**, *19*, 2867–2878. [CrossRef]
26. Yang, L.; Zhang, Y.; Zhang, M.; Liu, Y.; Bai, Z.; Ju, B. Modified flowing material balance equation for shale gas reservoirs. *ACS Omega* **2022**, *7*, 20927–20944. [CrossRef]
27. Zeng, J.; Liu, J.; Li, W.; Leong, Y.K.; Elsworth, D.; Guo, J. Shale gas reservoir modeling and production evaluation considering complex gas transport mechanisms and dispersed distribution of kerogen. *Pet. Sci. J.* **2021**, *18*, 195–218. [CrossRef]
28. Palmer, I.; Mansoori, J. How permeability depends on stress and pore pressure in coalbeds: A new model. *SPE Reservoir Evaluat. Eng.* **1998**, *1*, 539–544. [CrossRef]
29. Tanaka, E.; Inubushi, T.; Takahashi, K.; Shirakura, M.; Sano, R.; Dalla-Bona, D.A.; Nakajima, A.; van Eijden, T.M.G.J.; Tanne, K. Dynamic shear properties of the porcine molar periodontal ligament. *J. Biomech.* **2007**, *40*, 1477–1483. [CrossRef]
30. Karacan, C.Ö. Elastic and shear moduli of coal measure rocks derived from basic well logs using fractal statistics and radial basis functions. *Inter. J. Rock Mech. Sci.* **2009**, *46*, 1281–1295. [CrossRef]
31. Al-Qahtani, M.Y.; Zillur, R. A mathematical algorithm for modeling geomechanical rock properties of the Khuff and Pre-Khuff reservoirs in Ghawar field. *SPE Middle East Oil Show.* **2021**, *7*, 22–27.
32. Passey, Q.; Bohacs, K.; Esch, W.; Klimentidis, R.; Sinha, S. From oil-prone source rock to gas-producing shale reservoir–geologic and petrophysical characterization of unconventional shale-gas reservoirs. In Proceedings of the International Oil and Gas Conference and Exhibition in China, Beijing, China, 8–10 June 2010. [CrossRef]